CONF-9604120--2-Pt.1

WAPD-T-3095

CORROSION FATIGUE CRACK GROWTH IN CLAD LOW-ALLOY STEELS: PART I, MEDIUM-SULFUR FORGING STEEL

L. A. James, T. A. Auten, T. J. Poskie, and W. H. Cullen

U.S. Department of Energy Contract DE-AC11-93PN38195

DISCLAIMER

Proposed for Submittal to the
Journal of Pressure Vessel Technology

BETTIS ATOMIC POWER LABORATORY PITTSBURGH, PENNSYLVANIA 15122-0079

Operated for the U.S. Department of Energy
by WESTINGHOUSE ELECTRIC CORPORATION

WAPD-T-3095

CORROSION FATIGUE CRACK GROWTH IN CLAD LOW-ALLOY STEELS: PART I, MEDIUM-SULFUR FORGING STEEL

L. A. James*
Bettis Atomic Power Laboratory
West Mifflin, PA 15122

T. A. Auten
Knolls Atomic Power Laboratory
Schenectady, NY 12301

T. J. Poskie
Bettis Atomic Power Laboratory

and

W. H. Cullen
Materials Engineering Associates
Lanham, MD 20706

ABSTRACT

Corrosion fatigue crack propagation tests were conducted on a medium-sulfur ASTM A508-2 forging steel overlaid with weld-deposited Alloy EN82H cladding. The specimens featured semi-elliptical surface cracks penetrating approximately 6.3 mm of cladding into the underlying steel. The initial crack sizes were relatively large with surface lengths of 30.3-38.3 mm, and depths of 13.1-16.8 mm. The experiments were conducted in a quasi-stagnant low-oxygen (O_2 < 10 ppb) aqueous environment at 243°C, under loading conditions (ΔK, R, and cyclic frequency) conducive to environmentally-assisted cracking (EAC) in higher-sulfur steels under quasi-stagnant conditions. Earlier experiments on unclad compact tension specimens of this heat of steel did not exhibit EAC, and the present experiments on semi-elliptical surface cracks penetrating cladding also did not exhibit EAC.

INTRODUCTION

There has been considerable research interest in the environmentally-assisted cracking (EAC) response of low-alloy ferritic steels ever since Kondo et al. (1972) demonstrated that EAC could occur in a high-sulfur ASTM A302-B steel in a water environment at 260°C. Since that time, hundreds of research papers have addressed EAC, and the causes of the phenomenon are now reasonably well understood. The consensus view is that a critical crack-tip concentration (probably about 5 ppm) of sulfide (S^{2-}) or hydrosulfide (HS^-) ions is required to initiate EAC. The source of the sulfides may be either the water or the steel itself. However, in lieu of water-borne sulfide contamination, the only source of sulfides is metallurgical sulfide inclusions (e.g., MnS, FeS, etc.) that are embedded within the steel. The crack tip is therefore supplied with sulfides as the growing crack intersects the embedded sulfide inclusions and they dissolve in the presence of the elevated temperature water environment.

---

* Fellow ASME

Sulfides can be removed from the crack-tip region by any one, or more, of four mass-transport processes: 1) diffusion due to a concentration gradient, 2) ion migration due to a electrochemical potential (ECP) gradient, 3) fatigue "pumping" due to cyclic motion of the crack flanks, and 4) fluid flow induced within the crack cavity due to the presence of free stream fluid flow external to the crack. EAC initiates when the supply of sulfide ions to the crack tip exceeds the loss of sulfides through mass-transport for a sufficient period of time such that the critical crack-tip concentration is reached or exceeded.

Because the occurrence, or nonoccurrence, of EAC is the outcome of the competition between the supply of sulfides to the crack tip versus the loss of sulfides therefrom, factors that influence either the supply or loss can have a profound effect upon the outcome. For example, high sulfur content of the steel can enhance sulfide supply to the crack tip, while high free stream water flow rates parallel to the length of the crack can significantly enhance the loss of sulfides from the crack-tip region (James et al. 1995a, 1996). Similarly, elevated levels of dissolved oxygen (DO) in the bulk water environment can create an ECP gradient within the crack that tends to concentrate sulfide ions at the crack tip (Andresen and Young, 1995). These factors can operate singly or in concert to determine whether or not EAC will initiate.

Most of the EAC studies to date have been conducted employing test specimens similar to the compact tension (CT) specimen. From the above discussion it may be seen that mass-transport of sulfides from the crack-tip region is a very important consideration, and James et al. (1996) have suggested that mass-transport from a CT specimen may be different than mass-transport from a more prototypic semi-elliptical surface crack. Not only can sulfides be transported out along the sides of a crack in a CT specimen, but the crack-mouth opening displacement of a CT specimen is over twice that in a semi-elliptical surface crack of the same depth and loaded to the same level of stress intensity factor, K (James et al., 1996). Because of their more prototypic nature, this study will utilize semi-elliptical surface cracks.

Most of the EAC studies to date have been conducted on test specimens composed entirely of low-alloy steel. However, some applications may involve a layer of corrosion resistant cladding that is overlaid on the steel. A few studies have dealt with a crack penetrating a layer of cladding into the underlying steel. Pedron et al. (1984) studied the behavior of fatigue cracks penetrating weld-deposited austenitic stainless steel (SS) cladding into ASTM A508-2 steel in both air and vacuum environments at 300°C. Rahka et al. (1990) studied the behavior of fatigue cracks penetrating weld-deposited SS cladding into low-alloy steels in both low-DO (PWR) and high-DO (BWR) environments at 270° and 288°C, respectively. Bramwell et al. (1995) also studied fatigue cracks penetrating weld-deposited SS cladding into low-alloy steel in low-DO (PWR) water at 288°C. Finally, Ruther et al. (1991) studied the static-load crack growth behavior of a crack penetrating weld-deposited Alloy 182 cladding into A533-B steel in high-DO (BWR) water at 289°C. The objective of the three studies conducted in aqueous environments was to assess any possible galvanic effects due to the dissimilar metal couple. However, none of the earlier studies employed the more prototypic surface crack configuration. Therefore, the objective of this phase of the work was to study the fatigue crack propagation behavior of semi-elliptical surface cracks penetrating weld-deposited cladding into a medium-sulfur ASTM A508-2 steel. A second phase, presented in Part II, studied flow rate effects on surface cracks penetrating cladding into a high-sulfur steel.

EXPERIMENTAL PROCEDURE

Materials

The low-alloy steel employed in this phase was a medium-sulfur ASTM A508-2 (UNS K12766) forging. Two specimens were tested, and were given the designations "OV1" and "OU4". The chemical composition is given in Table I. Sulfur and nitrogen analyses were also made on material removed from each specimen at the completion of testing. Sulfur levels were 0.007% and 0.008% for Specimens OV1 and OU4, respectively. Nitrogen content was 0.004 percent by weight for both specimens. This same heat of steel (Heat 125H310VA1) has been employed in an earlier study utilizing unclad CT specimens in low-DO water at 149°C and 260°C (Forging "B" in Auten et al., 1993).

Two cladding processes were employed in the preparation of the specimens. A shielded-metal-arc (SMA) process was employed for Specimen OV1, and a gas-metal-arc (GMA) process was employed for Specimen OU4. Alloy EN82H (UNS N06082) filler metal was employed for both welding processes. The chemistries of the SMA electrode and the GMA wire are given in Table I. Following these weld-deposition processes, the cladding was machined to a uniform 6.35 mm depth. The cladding processes had introduced a strong residual magnetism in the low-alloy steel, and this was reduced by passing the weldments through degaussing coils. A piece of wrought Alloy 600 (UNS N06600) of sufficient size to allow the machining of the specimens was then joined to the Alloy EN82H by electron beam (EB) welding. The completed weldment assembly was then given a heat treatment at 607°C for 24 hours. The completed A508-2/Alloy EN82H/Alloy 600 specimen is illustrated in Figure 1.

Water Chemistry and Autoclave Conditions

Deaerated water containing 35-40 ml H_2/kg H_2O was employed in this study. Dissolved O_2 was therefore generally less than 10 ppb. The room temperature pH was about 10.2, while the calculated* pH at the test temperature of 243°C was 7.8. The room temperature conductivity was about 40 μS/cm. The electrochemical corrosion potential (ECP) of the specimen was measured during each test using a Ag/AgCl reference electrode. The relationship of Macdonald et al. (1979) was used to correct Ag/AgCl measurements to Standard Hydrogen Electrode (SHE) conditions. The autoclave volume was approximately 19 liters, and the water refreshment rate was approximately 50 ml/minute. Hence, on the average, about 6.3 hours would be required for one volume change of water; i.e., quasi-stagnant flow conditions.

Specimen Design

Because of the important role that the mass-transport of sulfides plays in EAC susceptibility, a specimen employing a semi-elliptical surface crack was utilized in this study. This specimen, described in more detail by James and Wilson (1994a), features a tight "natural" intersection of the crack with the free surface. There are no notches nor crack-starter slits to "short circuit" the mass-transport of sulfide ions from the crack enclave. Hence, the mass-transport paths are more prototypic than in CT specimens. The K-solution of Newman and Raju (1984) was employed to analyze the results.

---

*Calculated using MULTEQ (Electric Power Research Institute, Palo Alto, CA).

RESULTS AND DISCUSSION

Electrochemical Results

As stated earlier, the ECP was measured during testing employing a Ag/AgCl reference electrode. The reference electrode for the experiment on Specimen OV1 failed soon after the ascent to the test temperature of 243°C, but was measuring -727 mV_{SHE} at the time of failure. The results for the reference electrode employed on the experiment on Specimen OU4 are plotted in Figure 2. Three measurements were made throughout the test period (approximately 594 hours): Specimen OU4, an insulated coupon of the same steel, and an insulated platinum wire. Neither Specimen OV1 nor OU4 was electrically isolated from the loading system. However, as may be seen in Figure 2, there is essentially no difference between the ECP measured on Specimen OU4 and the free corrosion potential measured on the insulated steel coupon and the insulated platinum wire. The mean ECP of Specimen OU4 was -749 mV_{SHE} over the entire test period. This is in good agreement with the measurement at 243°C for several low-alloy steels in low-DO water reported by James (1994b), and the values of ECP reported in Part II of this paper.

The above ECP measurements on low-alloy steels are somewhat more active (electronegative) than values reported by James and Mills (1995b) for wrought Alloy 600 tested under similar conditions. The mean ECP for the Alloy 600 was approximately -660 mV_{SHE}. The Alloy 600 studied by James and Mills has a composition similar to that of the Alloy EN82H employed in the present study. This might tend to suggest that a potential gradient could have existed between the weld-deposited EN82H and the A508-2 steel in the present experiments. However, the specimen ECP measurements reported by James and Mills were for specimens that were not electrically isolated from the loading system; hence, they were not free corrosion potentials. In addition, as will be shown in Part II of this paper, free corrosion potential measurements on insulated coupons of Alloy 600 and A508-2 steel are virtually identical under both quasi-stagnant as well as high flow conditions. This result indicates that under the conditions that these tests were performed, the open-circuit potential is most likely controlled by the cathodic reaction, and the ECP difference between the steel and Alloy EN82H is small. Therefore, although a potential gradient from the Alloy EN82H to the A508-2 steel could influence mass-transport by ion migration, it is doubtful that a dissimilar metal couple would produce a potential gradient that was sufficient to induce ion migration in the present experiments in low-oxygen water. This, however, may not be the case for clad applications in high-DO water. Rahka et al. (1990) observed higher fatigue crack propagation (FCP) rates in a clad specimen tested in a high-DO BWR environment at 270°C than in an unclad specimen tested under similar conditions.

Fatigue Crack Growth Results

Specimens OV1 and OU4 were tested in low-DO water at 243°C. The maximum fatigue stress (membrane plus bending) at the free surface was 106.8 MPa, with a stress ratio ($R = \sigma_{max}/\sigma_{min}$) of 0.175. A cyclic frequency of 5.62 X 10^{-3} Hz was employed for both tests. A sawtooth load waveform was utilized that featured a load rise-time t_r = 151.5 seconds. Specimen OV1 was tested for 10,010 fatigue cycles, while Specimen OU4 was tested for 12,010 fatigue cycles. Specimen OU4 had an initial crack size of depth a = 13.08 mm and length 2c = 30.25 mm. Specimen OV1 featured a somewhat larger initial crack with depth a = 16.76 mm and length 2c = 38.28 mm.

No active measurements of crack extension were made during each test. At the completion of testing, the specimens were removed from the autoclave and then fractured following a soak in liquid nitrogen. Crack growth rates were then calculated using the "secant method"

and employing post-test measurements from the fracture surface; $da/dN \approx \Delta a/\Delta N$ and $dc/dN \approx \Delta c/\Delta N$. Post-test photomacrographs of the fracture surfaces are shown in Figure 3.

Crack growth results for Specimens OV1 and OU4 are plotted in Figure 4 using the "time-domain" format first suggested by Shoji et al. (1981, 1983). In this format, the ordinate ($\dot{a}_e$) is the experimentally-observed value of da/dN divided by the load rise-time, t_r. The abscissa ($\dot{a}_b$) is the mean value of da/dN expected for a low-alloy steel of this type in an air environment at that value of ΔK and R, again divided by t_r. In this case, the relationship developed by Eason et al. (1989) for A508-2 and A533-B steels in air was utilized.

The interpretation of the results for Specimen OU4 is straightforward. The Δa of 1.539 mm divided by ΔN of 12,010 produces an average crack growth rate $da/dN = 1.28 \times 10^{-4}$ mm/cycle, and dividing by t_r becomes $\dot{a}_e = 8.46 \times 10^{-7}$ mm/second. The average ΔK at the deepest penetration (Point "A") was 22.15 MPa$\sqrt{m}$ corresponding to $\dot{a}_e = 3.30 \times 10^{-7}$ mm/second. As shown in Figure 4, this plots quite close to the mean non-EAC line developed by James (1994b).

Interpretation of the results for Specimen OV1 is complicated by the fact that, as shown in Figure 3, the crack propagated to the edges of the specimen. Hence, the specimen at the later stages of the experiment was no longer a surface-crack specimen, but began to resemble a through-cracked specimen with an uneven (or "tunnelled") crack front. Uneven or tunnelled crack fronts are observed on occasion when conducting fracture toughness tests using CT or three-point-bend specimens, and several investigators have addressed such effects: e.g., see Towers and Smith (1984), Luchi and Rizzuti (1987), Yamamoto et al. (1987), Crouch (1991), and Kan and Blackburn (1992). Most of these studies have shown that if an "average" crack depth is assumed in the analysis, the resulting error is often within several percent. Therefore, the K-solutions from Tada (1985) for a through crack in a rectangular beam under uniform tension and for a through crack in a rectangular beam under pure bending were utilized. (See James and Wilson, 1994a, for a stress analysis of the specimen). Superposing these K-solutions and assuming an average crack depth (based on a nine-point average), the ΔK at the end of the experiment was estimated to be 39.15 MPa$\sqrt{m}$. The Newman and Raju (1984) solution for Point "A" on the initial semi-elliptical surface crack was estimated to be 31.17 MPa$\sqrt{m}$. Therefore, the average of the initial and final K-levels is 35.16 MPa$\sqrt{m}$ and this corresponds to a mean value of $\dot{a}_b = 1 \times 10^{-6}$ mm/second. The measured Δa at Point "A" was 2.54 mm, and when divided by ΔN = 10,010 cycles, da/dN became 2.54×10^{-4} mm/cycle. This corresponds to $\dot{a}_e = 1.67 \times 10^{-6}$ mm/second. Although this treatment of the results for Specimen OV1 is not completely rigorous, the results do indicate that EAC was not observed in either Specimen OU4 or OV1.

It is also possible to evaluate the results of the experiments on Specimens OV1 and OU4 by comparing the actual observed post-test crack dimensions to those predicted assuming either EAC or non-EAC conditions in the steel. The predictions were made by numerically integrating the fatigue crack growth equation(s) on a cycle-by-cycle basis using the K-solution of Newman and Raju (1984). The appropriate crack growth equations were employed at Point "C" on the surface (EN82H relationship per James and Mills, 1995b, see Figure 5), and at Point "A" at the deepest penetration (A508-2 relationships for EAC and non-EAC per James, 1994b). The comparison between predicted and actual crack dimensions are shown in Figures 6 and 7 for Specimens OV1 and OU4, respectively, and in both cases it is clear that the final post-test crack dimensions are much closer to the predictions using mean non-EAC properties. These agreements are considered quite good considering the complicating factors involved in such predictions: 1) the different crack growth relationships at Points "A" and "C", 2) welding residual stresses within the cladding (these relax away with

the growth of the crack), 3) stress differentials across the cladding/base metal interface due to differences in the coefficients of thermal expansion (tensile in the EN82H and compressive in the steel, these do not relax away with the growth of the crack), 4) the usual $r^{-0.5}$ crack-tip singularity becomes $r^{\lambda-1}$ (where $0 < \lambda < 1$, λ is a function of the crack geometry and the four elastic constants) when the crack tip approaches (Romeo and Ballarini, 1995) or reaches (Lin and Mar, 1976) the bimetallic boundary, and 5) the usual $r^{-0.5}$ crack-tip singularity is not present at the intersection of the crack and the free surface at Point "C" (Bažant and Estenssoro (1979), Sih and Lee (1989), and Pook, (1994)).

This same heat of A508-2 steel was employed in an earlier study by Auten et al. (1993) utilizing unclad CT specimens in low-DO water at 260°C. These results are also plotted in Figure 4 for comparison, and again EAC was not observed. There is good agreement between the results for the two specimen types.

The results on Specimen OU4 also allow the opportunity to check the FCP rate observed at the surface of the semi-elliptical crack (Point "C") against earlier results for CT specimens composed entirely of Alloy EN82H and tested under similar conditions (James and Mills, 1995b). The change in crack length for the experiment on Specimen OU4 was $\Delta 2c = 6.30$ mm, resulting in a crack growth rate $dc/dN = 2.62 \times 10^{-4}$ mm/cycle at an average ΔK of 26.23 MPa$\sqrt{m}$. As shown in Figure 5, this result compares favorably with the previous results of James and Mills.

Finally, it will be observed in Figure 3 that, at the time of the end of the test on Specimen OU1, the crack had not propagated beyond the clad/base-metal interface at the sides of the specimen. Other investigators have also observed that the crack is either temporarily retarded or the FCP rates are temporarily reduced as the crack reaches the clad/base-metal interface; e.g., see Rahka et al. (1990) and Bramwell et al. (1995). This is because the difference in the coefficients of thermal expansion between the cladding material and the low-alloy steel sets up a local tensile stress in the cladding and a local compressive stress in the steel. This local compressive stress temporarily reduces the FCP rate at the interface. However, unless the applied stress range is quite low, the retardation is only temporary as evidenced by the fact that fatigue cracks did penetrate the cladding/base-metal interface in the studies by Rahka et al. and Bramwell et al., as well as in Part II of the present paper. (See also the studies on underclad cracking by Bernard et al., 1992).

SUMMARY

FCP experiments were conducted on two specimens where a semi-elliptical surface crack penetrated approximately 6.35 mm of weld-deposited cladding into the underlying medium-sulfur A508-2 steel. The experiments were conducted at 243°C in low-DO water under loading conditions (ΔK, R, t_r) conducive to EAC in high-sulfur steels. However EAC was not observed in either specimen, and this is in agreement with results from previous experiments on the same heat of steel utilizing unclad CT specimens. Hence, the presence of the cladding does not appear to introduce any factors that would increase the susceptibility of these medium-sulfur steels to EAC in low-DO water. In addition, the surface-crack configuration produced results that were equivalent to those observed previously with CT specimens; EAC was not observed with either specimen design.

ACKNOWLEDGEMENTS

This work was performed under a U. S. Department of Energy contract with the Bettis Atomic Power Laboratory, a unit of the Westinghouse Electric Corporation. The experimental work was conducted under a subcontract with Materials Engineering Associates of Lanham, MD.

REFERENCES

Andresen, P. L. and Young, L. M., 1995, "Crack Tip Microsampling and Growth Rate Measurements in Low Alloy Steel in High Temperature Water," *Corrosion*, Vol. 51, No. 3,, pp. 223-233

Auten, T. A., Hayden, S. Z., and Emanuelson, R. H., 1993, "Fatigue Crack Growth Rate Studies of Medium Sulfur Low Alloy Steels Tested in High Temperature Water," *Proceedings Sixth International Symposium on Environmental Degradation of Materials in Nuclear Power Systems - Water Reactors*, TMS-AIME, pp. 35-41

Bažant, Z. P. and Estenssoro, L. F., 1979, "Surface Singularity and Crack Propagation," *International Journal of Solids and Structures*, Vol. 15, No. 5, pp. 405-426

Bernard, J. L., Vagner, J., Pellissier-Tanon, A., and Fauer, F., 1992, "Effect of Residual Stresses and Complex Loadings on the Fatigue Behavior of Underclad Cracks," *Nuclear Engineering and Design*, Vol. 133, No. 1, pp. 3-15

Bramwell, I. L., Tice, D. R., Worswick, D., and Heys, G. B., 1995, "The Effect of Stainless Steel Overlay Cladding on Corrosion Fatigue Crack Propagation in a Pressure Vessel Steel in PWR Primary Coolant", *Proceedings Seventh International Symposium on Environmental Degradation of Materials in Nuclear Power Systems - Water Reactors,* Vol 2, NACE, 1995, pp. 1157-1168

Crouch, B. A., 1991, "The Effect of Crack Front Curvature and Side-Grooving on Three Point Bend Specimen Fracture Toughness Measurement", *International Journal of Fracture*, Vol. 52, No. 4, pp. 275-292

Eason, E. D., Andrew, S. P., Warmbrodt, S. B., Nelson, E. E., and Gilman, J. D., 1989, "Analysis of Pressure Vessel Steel Fatigue Tests in Air," *Nuclear Engineering and Design*, Vol. 115, No. 1, pp. 23-30

James, L. A., and Wilson, W. K. 1994a, "Development of a Surface-Cracked Specimen," *Theoretical and Applied Fracture Mechanics*, Vol. 20, No. 2, pp. 115-121

James, L. A., 1994b, "The Effect of Temperature and Cyclic Frequency Upon Fatigue Crack Growth Behavior of Several Steels in an Elevated Temperature Aqueous Environment," *Journal of Pressure Vessel Technology*, Vol. 116, No. 2, pp. 122-127

James, L. A., Wire, G. L., and Cullen, W. H., 1995a, "The Effect of Water Flow Rate Upon the Environmentally-Assisted Cracking Response of a Low-Alloy Steel," *Journal of Pressure Vessel Technology*, Vol. 117, No. 3, pp. 238-244

James, L. A., and Mills, W. J., 1995b, "Fatigue Crack Propagation Behavior of Wrought Alloy 600 and Weld-Deposited EN82H in an Elevated Temperature Aqueous Environment", *Service Experience, Structural Integrity, Severe Accidents, and Erosion in Nuclear and Fossil Plants,* ASME Publication PVP-Vol. 303, pp. 21-36

James, L. A., Lee, H. B., and Wire, G. L., 1996, "The Effect of Water Flow Rate Upon the Environmentally-Assisted Cracking Response of a Low-Alloy Steel: Experimental Results Plus Modeling", *Journal of Pressure Vessel Technology*, in press (WAPD-T-3067)

Kan, R., and Blackburn, W. S., 1992, "Effect of Crack Front Non-Linearity on Results From Compact Tension Tests", *International Journal of Fracture*, Vol, 55, No. 3 pp. 285-292

Kondo, T., Kikuyama, T., Nakajima, H., and Shindo, M., 1972, "Fatigue of Low-Alloy Steels in Aqueous Environment at Elevated Temperatures," *Mechanical Behavior of Materials, Proc. of International Conference on Mechanical Behavior of Materials*, Vol. 3, pp. 319-327

Lin, K. Y. and Mar, J. W., 1976, "Finite Element Analysis of Stress Intensity Factors at a Bimaterial Interface", *International Journal of Fracture*, Vol. 12, No. 4, pp. 521-531

Luchi, M. L., and Rizzuti, S., 1987, "Boundary Element Analysis of CT Specimens With Straight and Curved Crack Fronts", *International Journal of Fracture*, Vol. 34, No. 1, pp 23-40

Macdonald, D.D., Scott, A. C., and Wentrcek, P., 1979, "Silver-Silver Chloride Thermocells and Thermal Liquid Junction Potentials for Potassium Chloride Solution as Elevated Temperatures," *Journal of the Electrochemical Society*, Vol, 126, No. 9, pp. 1618-1624

Newman, J. C. And Raju, I. S., 1984, "Stress Intensity Factor Equations for Cracks in Three-Dimensional Finite Bodies Subjected to Tension and Bending Loads", NASA Technical Memorandum 85793

Pedron, J. P., Diboine, A., and Pineau, A., 1984, "Fatigue Crack Growth Rate Behavior of Stainless Steel Claddings in Air and Under Vacuum at 300°C," *Fatigue of Engineering Materials and Structures*, Vol. 7, No. 2, pp. 137-143.

Pook, L. P., "Some Implications of Corner Point Singularities, 1994," *Engineering Fracture Mechanics*, Vol. 48, No. 3, pp. 367-378

Rahka, K., Hänninen, H., Saario, T., Törrönen, K., and Ahlstrand, R., 1990, "Fatigue Crack Propagation Through Welded Cladding Into Base Metal in LWR-Pressure Vessel Materials," NUREG/CP-0112, Vol. 1, pp. 253-262

Romeo, A. and Ballarini, R., 1995, "A Crack Very Close to a Bimaterial Interface," *Journal of Applied Mechanics*, Vol. 62, No. 3, pp. 614-619

Ruther, W. E., Shack, W. J., Chung, H. M., Kassner, T. F., and Soppet, W. K., 1991, "Environmentally Assisted Cracking in Light Water Reactors", NUREG/CR-4667, Vol. 10

Shoji, T., Takahashi, H., Suzuki, M., and Kondo, T., 1981, "A New Parameter for Characterizing Corrosion Fatigue Crack Growth," *Journal of Engineering Materials and Technology*, Vol. 103, No. 4, pp. 298-304

Shoji, T., Takahaski, H., Nakajima, H., and Kondo, T., 1983, "Role of Loading Variables in Environment Enhanced Crack Growth for Water-Cooled Nuclear Reactor Pressure Vessel Steels," NUREG/CP-0044, Vol. 2, pp. 143-171

Sih, G. C. and Lee, Y. D., 1989, "Review of Triaxial Border Stress and Energy Behavior," *Theoretical and Applied Fracture Mechanics*, Vol. 12, No. 1, pp. 1-17

Tada, H., 1985, *The Stress Analysis of Cracks Handbook*, Second Edition, Paris Productions Inc., St. Louis

Towers, O. L., and Smith, A. P., 1984, "Stress Intensity Factors for Curved Crack Fronts in Compact Tension Specimens", *International Journal of Fracture*, Vol. 25, No. 2, pp. R43-R48

Yamamoto, Y., Sumi, Y., Shimoyama, T., and Funada, T., 1987, "On Thumb-Nail Pattern of Fatigue Crack Front Observed in Standard Compact Tension Specimen", *International Journal of Fracture*, Vol. 34, No. 2, pp. 149-157

WP:950280N.WP5

Table I

Chemical Compositions

Alloy	Heat No.	C	Mn	P	S	Si	Ni	Cr	V	Mo	Cu	Ti	Fe	Nb+Ta
A508-2	125H310VA1	0.21	0.65	0.008	0.012*	0.27	0.71	0.36	0.01	0.62	0.05	-	Balance	-
EN82H (SMA)	ET5891	0.03	5.9	-	0.005	0.7	Balance**	15.0	-	-	-	0.5	7.2	2.0***
EN82H (GMA)	NX4644DK	0.04	2.99	0.001	0.001	0.06	72.74****	19.81	-	-	0.02	0.43	1.38	2.53

*Vendor certified ladle sulfur analysis = 0.012%
Statistics for nine additional sulfur analyses: range = 0.009-0.013%
mean = 0.0097%
std. dev. = 0.0013%

** Includes cobalt (Co = 0.03%)

*** Ta = 0.05%

**** Includes cobalt.

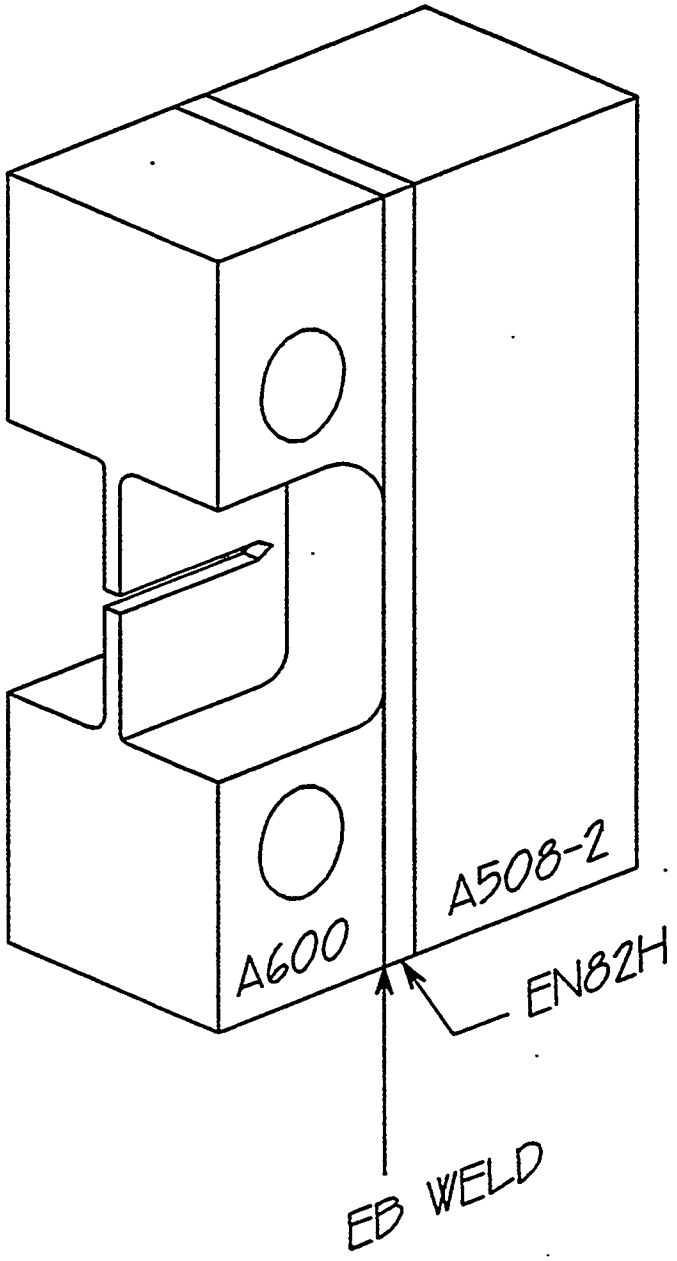

Figure 1 Schematic of the composite A508-2/EN82H/Alloy 600 specimen prior to the removal of the precracking web. See Figure 1 of Part II for the specimen with the web removed.

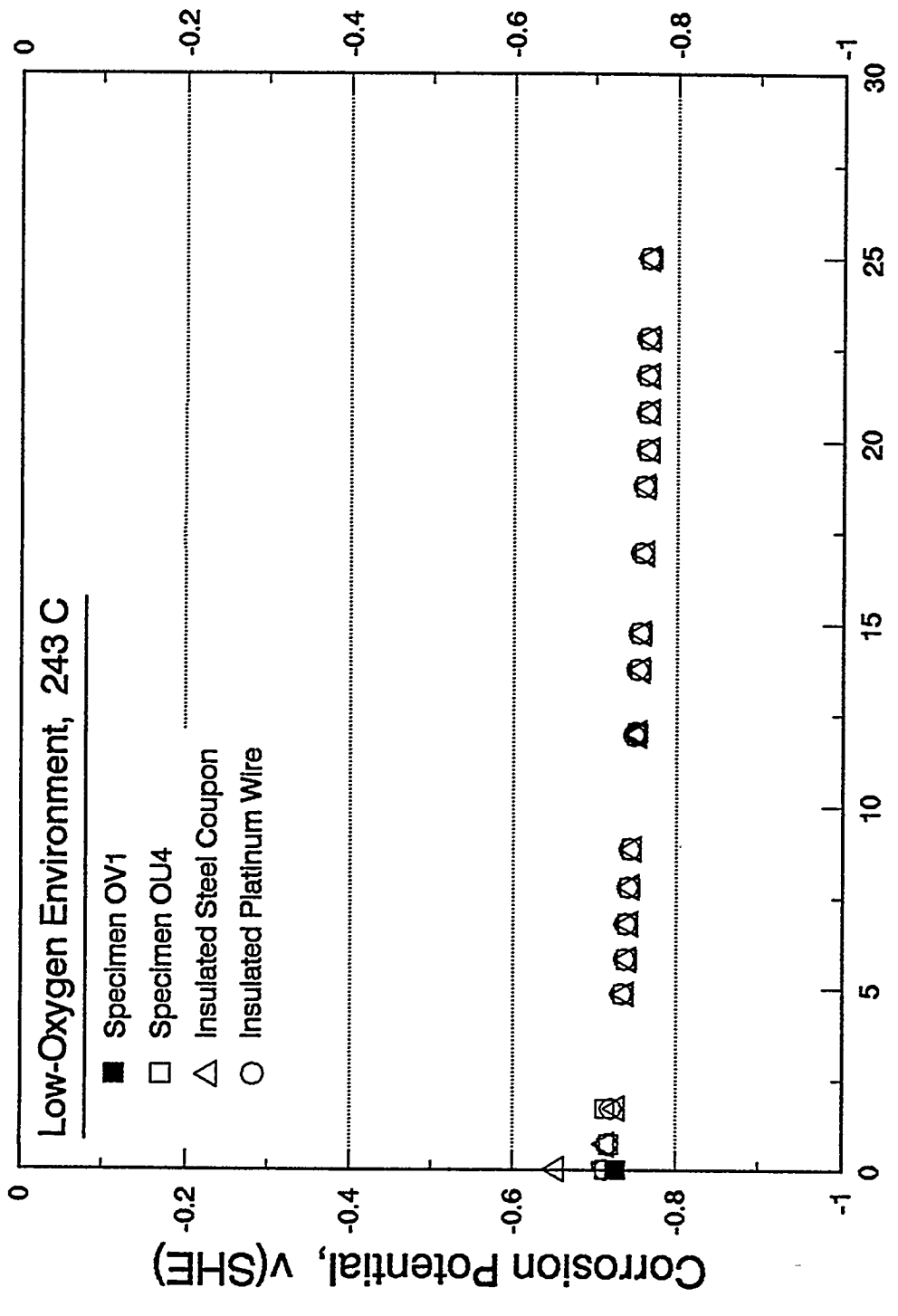

Figure 2 Corrosion potentials observed during the experiment on Specimen OU4 and the early portion of the experiment on Specimen OV1.

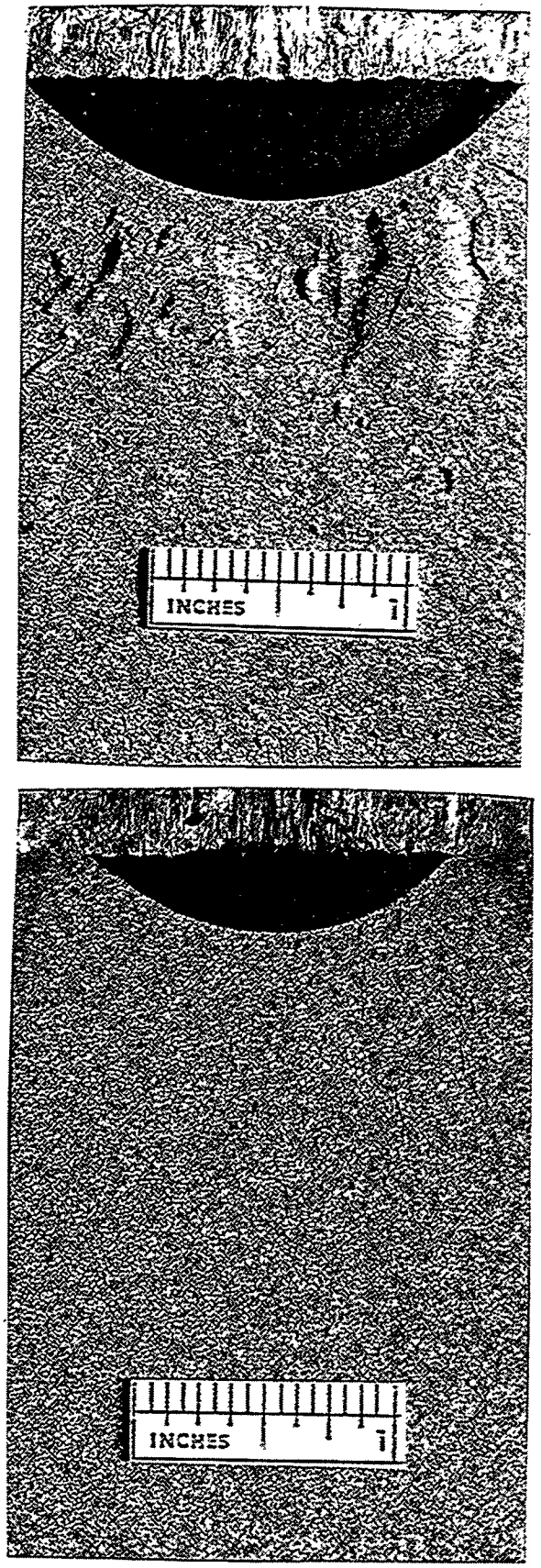

Figure 3 Post-test photomacrographs of the fracture faces of Specimen OV1 (top) and OU4 (bottom)

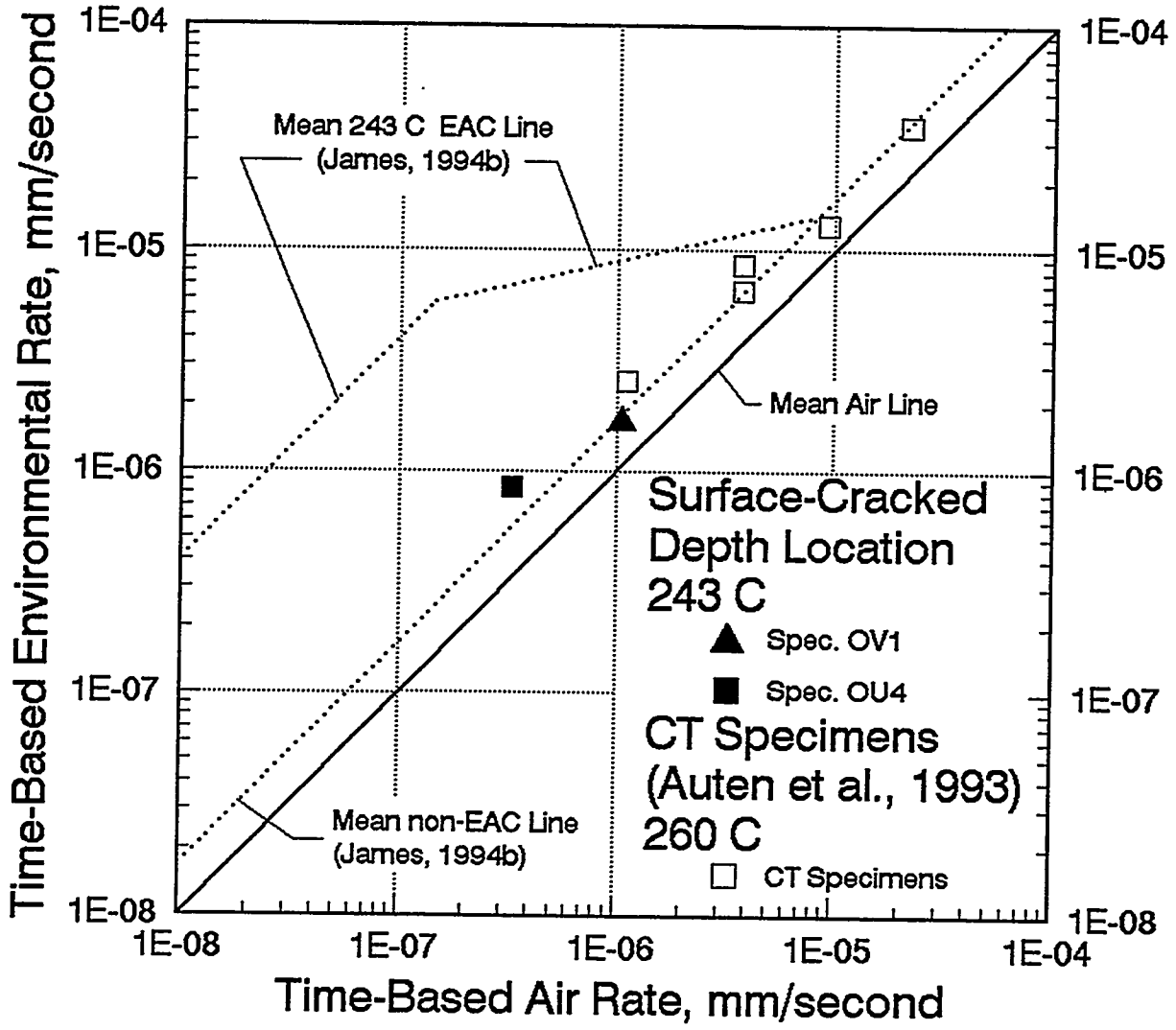

OU4C.DRW

Figure 4 Time-domain plot of the crack growth behavior into the depth direction of clad Specimens OV1 and OU4. Also shown are results for CT specimens from the same heat of steel tested at 260°C.

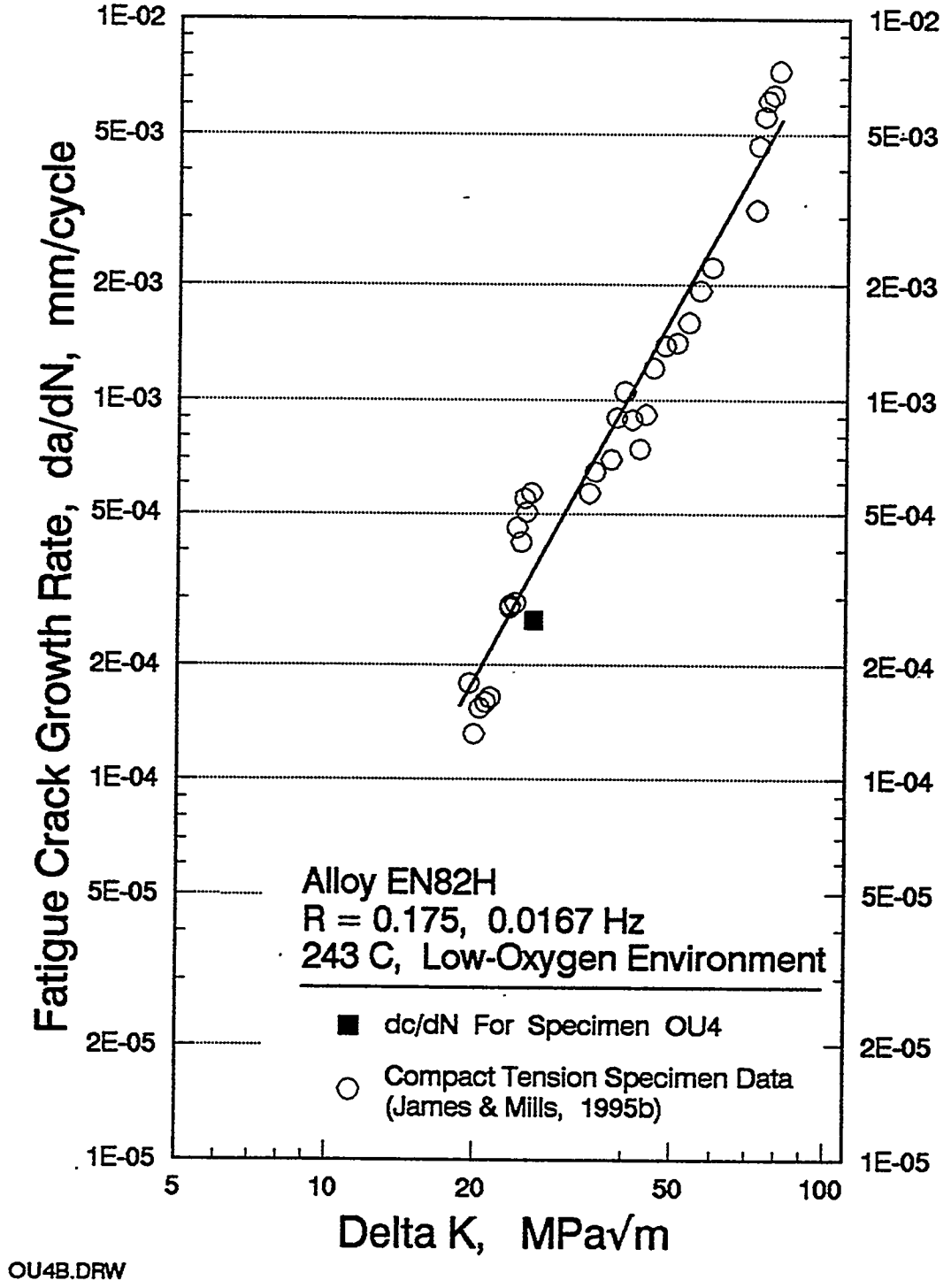

Figure 5 Fatigue crack growth behavior at the surface location (Point "C") of Specimen OU4 compared with results from James and Mills (1995b) employing compact tension specimens.

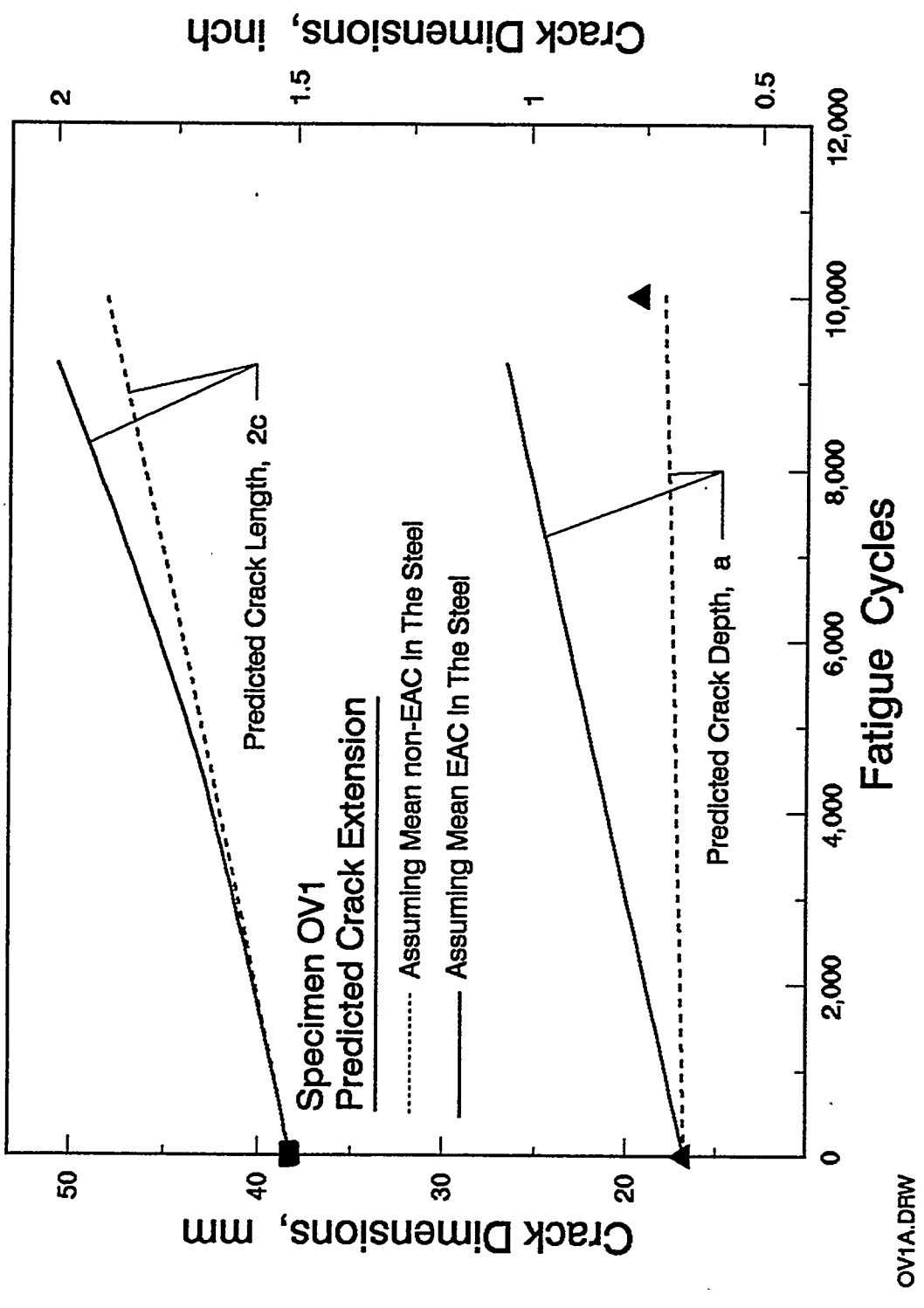

Figure 6. Crack growth predictions for Specimen OV1 for the two cases of mean non-EAC behavior and mean EAC behavior. The actual crack dimensions are shown as solid symbols.

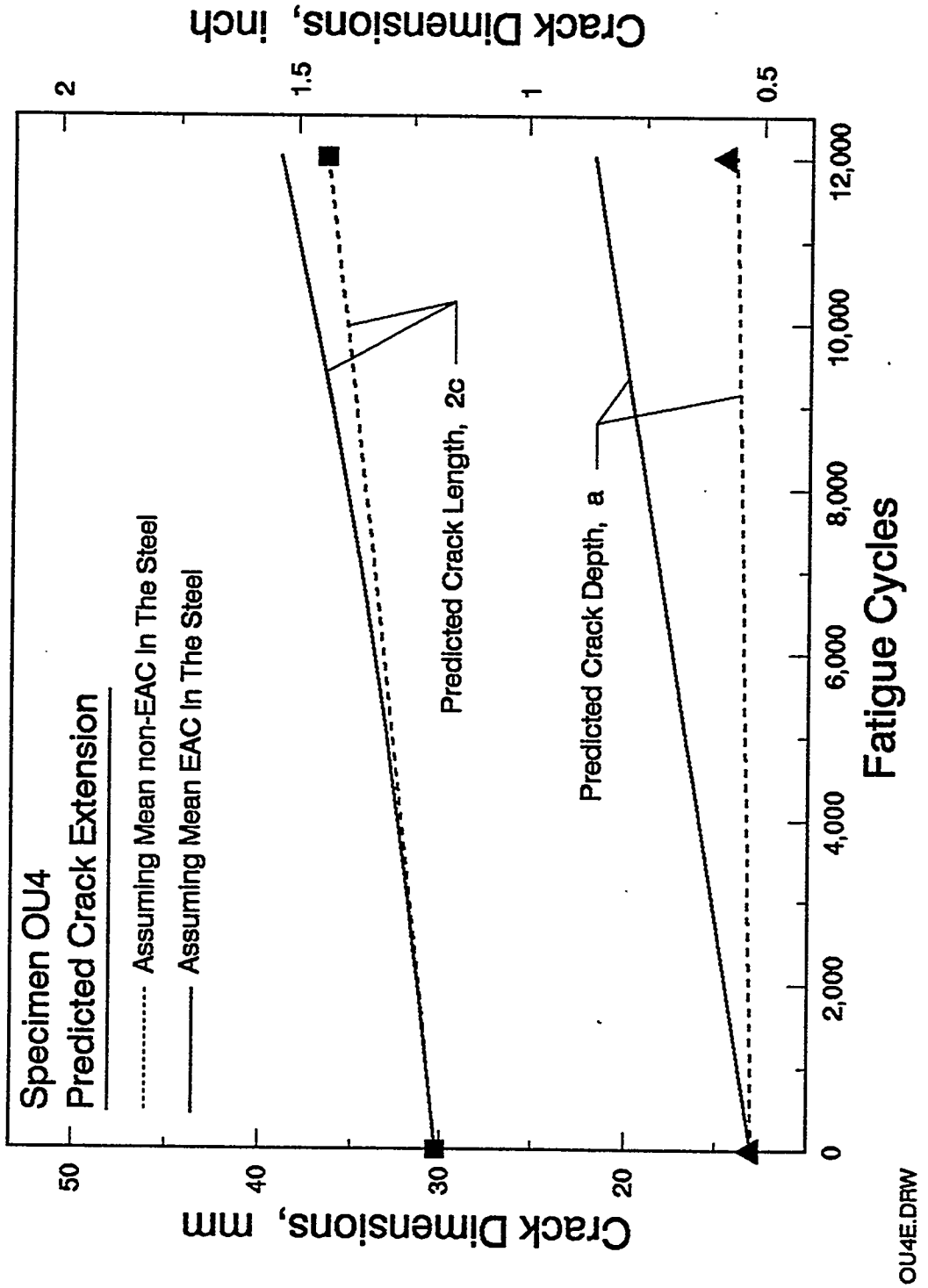

Figure 7. Crack growth predictions for Specimen OU4 for the two cases of mean non-EAC behavior and mean EAC behavior. The actual crack dimensions are shown as solid symbols.